Dynamical Effects and Product Distributions in Simulated CN + Methane Reactions

Thomas J. Preston[1], Balázs Hornung[1], Shubhrangshu Pandit[1], Jeremy N. Harvey[2], and Andrew J. Orr-Ewing[1,*]

[1] *School of Chemistry, University of Bristol, Cantock's Close, Bristol, BS8 1TS, UK.*
[2] *Department of Chemistry, KU Leuven, Celestijnenlaan 200F, B-3001 Leuven (Heverlee), Belgium.*

15 January 2016

* Author for correspondence

e-mail: a.orr-ewing@bristol.ac.uk

Tel: +44 1179287672

Abstract

Dynamics of collisions between structured molecular species quickly become complex as molecules become large. Reactions of methane with halogen and oxygen atoms serve as model systems for polyatomic molecule chemical dynamics, and replacing the atomic reagent with a diatomic radical affords further insights. A new, full-dimensional potential energy surface for collisions between CN + CH_4 to form HCN + CH_3 is developed and then used to perform quasi-classical simulations of the reaction. Coupled-cluster energies serve as input to an empirical valence bonding (EVB) model, which provides an analytical function for the surface. Efficient sampling permits simulation of velocity map ion images and exploration of dynamics over a range of collision energies. Reaction populates HCN vibration, and energy partitioning changes with collision energy. The reaction cross-section depends on the orientation of the diatomic CN radical. A two-dimensional extension of the cone of acceptance for an atom in the line-of-centers model appropriately describes its reactivity. The simulation results foster future experiments and diatomic extensions to existing atomic models of chemical collisions and reaction dynamics.

I. Introduction

The highly reactive cyanide radical, CN, presents a prime target for understanding chemical reaction dynamics on a fundamental level. It abstracts hydrogen atoms from hydrocarbons,[1-5] adds to unsaturated carbon-carbon bonds,[6-7] and is more electrophilic than Cl and F.[8] Because it behaves so similarly to F and Cl atoms, it is often convenient to consider CN as a *pseudohalogen*. Hydrogen-abstraction reactions with halogen atoms have been proving grounds for techniques and theories of bimolecular reactions for many years. Even seemingly simple reactions continue to surprise.[9] Exploring reactions with CN promises to add further to our understanding of these classes of bimolecular reactions.

The diatomic cyanide radical poses both extra constraints and possibilities, however, to the dynamics of these prototypical bimolecular reactions. Moving from a spherical atom to a non-spherical diatom introduces additional stereochemical constraints. Notions such as the cone of acceptance,[10-11] a powerful idea for halogen-atom reactions, warrant an update in orientation-dependent reactions with cyanide radicals. The CN can contain rotational and vibrational energy, which can influence reactivity. The HCN product has additional stretching and bending degrees of freedom that can soak up some of the exothermicity of the reaction. Reaction at the N end of the radical can also form hydrogen isocyanide, HNC. It is the goal of the current work to explore some, but not all, of these ideas in hydrogen abstraction from hydrocarbons by CN. In so doing, we build on our recent quantum-state-resolved dynamics measurements and simulations of halogen-atom reactions with saturated[12] and unsaturated polyatomic reactants in gas[13-14] and liquid phases.[15-17]

A lag exists in our understanding of the gas-phase CN hydrogen-abstraction dynamics relative to those in the condensed phase. Throughout the last 30 years of femtosecond laser studies, the research community has tended to adopt a from-gas-to-liquid-phase mentality in its construction of atom-by-atom descriptions of chemical reactions. With CN reactions, we are now in the curious position where the liquid-phase studies have outpaced those in gas phase.[18-24] Bulk gas-phase measurements are capable of monitoring HCN production from CN collisions with saturated hydrocarbons and provide an excellent starting point for interpreting the dynamics.[1-2, 25] Recent microwave spectra of collisionally cooled products of CN + propyne reactions highlight the large numbers of reaction pathways and the importance of decoupling the reaction mechanisms.[6] In single-collision experiments that use non-state-selective ionization to measure scattering of reaction products, parallels between Cl and CN mechanisms have been established.[4, 7, 26-28] Without state-resolved detection of the reaction products, ion-

imaging measurements provide qualitative descriptions of the reaction and the dynamical nuances of CN reactions remain opaque.

We target the reaction CN + CH_4 → HCN + CH_3 and its fully deuterated isotopologue as an entry point to state-resolved gas-phase studies for three main reasons. First, the relative simplicity of the reaction combined with the possibility of detecting both product fragments - HCN and CH_3 - with quantum-state-specificity present the opportunity to understand this reaction in detail. Second, as mentioned above, it is a relatively straight-forward first reaction for studying bimolecular CN reactions in the gas phase. Third, the exothermicity of the reaction[2]

$$CN + CH_4 \rightarrow HCN + CH_3 \qquad \Delta_r H_{0\,K} = -87 \text{ kJ/mol}$$

deposits large amounts of energy in the fragments, allowing us to make useful, dynamical predictions. In contrast with H abstraction from larger alkanes,[1, 18] there is a barrier to H abstraction of about 9 kJ/mol.[2, 5, 29]

The empirical valence bonding method[30-31] allows us to build a full-dimensional potential energy surface for the title reaction. The EVB method requires only a modest number of *ab initio* calculations to produce reliable surfaces for efficiently propagating quasi-classical collisions.[32] We have shown the utility of these surfaces in Cl + methane[12] and Cl + propene[14] gas-phase reactions and CN + alkane liquid-phase reactions,[18-20, 22] but now demand the methodology to lead rather than follow our experimental undertakings. Such studies step beyond simple assessments of minimum-energy pathways and inspect the role of dynamics as fragments collide to effect chemical transformation.

II. Calculations

There are three sequential steps in this work for simulating the reaction dynamics of CN + methane collisions: developing the potential energy surface, propagating quasi-classical

trajectories, and analyzing the results of reactive encounters. Throughout this work we ignore HNC production, and doing so has little effect on our dynamics because the barriers to direct production by N-end approach and isomerization from HCN[33-34] are much higher than the energies we consider here.

A. Potential Energy Surface

Warshel and Weiss developed the empirical valence bonding (EVB) model to describe a reactive potential energy surface using chemically intuitive coordinates.[30] In EVB, energies, and by differentiation, forces on the atoms come from a force field of additive functions of molecular motions: bond stretches, angle bends, dihedral-angle bends, and out-of-plane distortions. Further additive terms for intermolecular van der Waals energies describe long-range attraction and short-range repulsion. For CN reaction with CH_4, the reactant and four equivalent product force fields, one for each H atom, form five basis states along the diagonal of the EVB matrix. Simple geometric functions of the bond-breaking and -forming distances, which we describe in the Supporting Information, couple the reactants and products. We have applied this technique to both gas- and liquid-phase reactions previously, showing excellent agreement with experimental results.[12, 14, 22, 30, 32] Most of the procedures we use for fitting the $CN + CH_4 \rightarrow HCN + CH_3$ surface have direct analogies to building our $Cl + CH_4$ EVB surface.[12]

Fitting the reactive surface begins with fitting intramolecular parameters for separated molecular species: CN, CH_4, HCN, and CH_3. For example, exploring the two bond-stretching terms and one angle-bending term for HCN involves performing three separate rigid scans along the C-H and C-N stretching and HCN bending coordinates. In each rigid scan, the remaining internal coordinates are set to their equilibrium values. In this work, Morse functions describe bond stretching, and harmonic functions describe angle bending and Wilson-type out-

of-plane bending. Minimizing the root-mean-square deviation between the force-field and the *ab initio* energies generates the parameters for each term.

We opt for unrestricted coupled-cluster calculations using unrestricted Hartree-Fock reference wavefunctions (UCCSD-UHF) with Dunning's cc-pVDZ basis set. Glowacki and co-workers showed that reliable reaction energies for CN reactions with propane could be obtained using UCCSD/cc-pVDZ optimized geometries along the reaction coordinate and single point energies from UCCSD(T) calculations extrapolated from cc-pVDZ and cc-PVTZ basis sets to the infinite basis set limit.[18] We have modified that methodology by including diffuse functions with the aug-cc-pVDZ basis set and by omitting perturbative triple excitations and extrapolation to the complete basis-limit. This methodology satisfactorily reproduces the experimental value for the exothermicity of the reaction at 0 K (see Section III). We estimate the error due to basis-set superposition to be about 6 kJ/mol near the transition state, and about 1 kJ/mol in the entrance and exit valleys using the counterpoise method. All electronic structure calculations use Gaussian09.[35] The barrier height of 11 kJ/mol on the uncorrected surface recovers the experimentally determined barrier of about 9 kJ/mol, [2, 5] but this comparison neglects zero-point vibrational energy effects. Omitting the counterpoise correction in the *ab initio* calculations we use for the EVB fit will not change the general conclusions herein, and we use a PES that is not corrected for BSSE. Continuing the example of HCN from the previous paragraph, the preliminary C-H and C-N stretching and HCN bending parameters are used as initial guesses to fit all three dimensions simultaneously over random geometries in the dynamically relevant 0-90 kJ/mol energy range. The extracted parameters change only a few percent from their original values and the average error per *ab initio* point changes less than 1 kJ/mol relative to the original fit. We subject each molecular species, CN, CH_4, HCN, and CH_3, to appropriate scans and fitting. Intramolecular parameters from these separated scans remain

fixed in further fitting to the reactive surface. The Supporting Information contains the functions and the fitted parameters for the surface.

Following our recent work using EVB surfaces to study Cl + hydrocarbon reactions[12, 14] we use the four-parameter Buckingham-Corner potential to describe van der Waals interactions between molecular fragments.[36] The initial parameters come from the CH_4 + Cl potential,[12] adopting C values for N. The fitted parameters and the functional form, which is sufficiently flexible without introducing over-fitting to the *ab initio* points, are given in the Supporting Information.

A two-dimensional, tilted elliptical Gaussian couples the reactants and products. The Supporting Information gives the functional form and fitted parameters. It is the same type of coupling function as we have used[14] for H abstraction from propene by Cl atoms. In CN + CH_4, the coupling Gaussian takes the H_3C-HCN and H_3CH-CN distances as its arguments. Fitting optimizes the amplitude, center, widths of the major and minor axes, and angle between the axis of the coupling term and breaking bond. The coupling term ignores the position of the N atom, meaning that coupling strength is independent of the H-C-N angle. The EVB surface, however, faithfully represents the UCCSD energies with bent HCN geometries. We make lengthy discussion of the importance of this angle on the surface and the dynamics in Sec III, which shows the omission of this coordinate in the coupling term is valid.

Two-dimensional scans of the H_3C-HCN and H_3CH-CN bond distances of the full CH_4-CN system in C_{3v} geometries, with all other coordinate optimized, provide *ab initio* energy values for initial fitting to the hydrogen-transfer region. Preliminary explorations showed that optimized geometries in the UHF framework are displaced from the UCCSD geometries. Thus, we first used the modified BB1K/6-31G(d) prescription put forth earlier[18] to optimize geometries and then calculated UCCSD-UHF/aug-cc-pVDZ energies for those geometries for fitting the EVB surface.

Initial estimates for all parameters in hand, we fit the surface to the scanned *ab initio* points over the entrance valley, H-transfer region, and exit valley. This fit provides the preliminary surface that we use to run trial reactive trajectories from which we extract dynamically relevant structures and their energies. Randomized geometries are extracted from 1200 trajectories throughout the reaction path, but we ensure good coverage of important geometries. The 340 scanned and 430 dynamical geometries constitute the set for the final fit. Parameters for isolated molecules stay fixed, but coupling and van der Waals parameters vary for the final fit. The average unsigned deviation between the UCCSD-UHF and EVB energies over these 770 geometries is 3.4 kJ/mol in the -50 to 90 kJ/mol range. As a check on the goodness of the fit, we propagate several trajectories and extract randomized geometries from the entrance and exit channels and the H-transfer region. These 100 new, unfit, dynamical geometries produce an average error of 3.9 kJ/mol relative to the UCCSD-UHF energies.

B. Trajectories

We propagate classical trajectories using VENUS[37-39] interfaced with an EVB module developed in our group. Simulations start with 5 Å separating the carbon atoms of CH_4 and CN, a choice guided by our recent Cl-atom reaction studies.[12, 14] This initial separation is ≥ 1 Å larger than the maximum impact parameter for reaction and lies beyond the strongly interacting region of the PES, but also represents a compromise for computational efficiency. Trajectories terminate when the departing H is 7 Å from the methyl C, and use a 0.1 fs timestep for propagation, which we have shown sufficiently conserves energy and angular momentum for similarly exothermic reactions.[14] Methane and cyanide start with random orientations, vibrational energy equal to their zero-point values (with sampling from a 0 K Boltzmann distribution of normal mode energies), and zero rotational energy unless otherwise stated. Only reactions that have at least zero-point vibrational energy in both products qualify as successful.

The modest barrier and favorable energy partitioning lead to reasonable production rates (e.g. fewer than 50% of reactive CN + CH_4 trajectories were rejected for collision energies ≥ 20 kJ/mol, and acceptance rates were higher for CN + CD_4). Impact parameters (defined with respect to the centers of mass of CN and methane) were sampled in VENUS up to a maximum value, b_{max}. We set this b_{max} cutoff by inspecting the opacity function and using the value of b such that 99.5% of all reactive trajectories are included within the sampling bounds. In principle, b_{max} is a function of E_{coll} but we find it varies only a little for our simulations; we use b_{max} = 3.5 Å for $E_{coll} \geq 9.9$ kJ/mol and b_{max} = 4.0 Å for $E_{coll} \leq 5.6$ kJ/mol. The chosen sampling of initial conditions and the large numbers of trajectories propagated (see below) ensure that the QCT calculations provide a fair simulation of future experiments.

One intention of the current work is to predict the results of the title reaction under experimentally relevant conditions. The efficiency of both the EVB method and the relative simplicity of the reaction itself allow us to simulate it over a range of initial conditions. The current simulations are designed for comparison with future experiments using a molecular-beam machine, which has a tunable collision energy E_{coll}. Thus, we attempt to span a reasonable portion of the expected parameter space in our simulations; the collision energies we study reflect experimentally tenable conditions. **Table I** collects the pertinent initial conditions for the simulations we have performed and reports the numbers of trajectories propagated and that led to reaction.

TABLE I: Initial Conditions and Numbers of Simulations for CN + Methane Reactions

CN rotational quantum number	colliding partner	collision energy (kJ/mol)	collisions simulated / 10^6	total reactions	accepted reactions[a]
0	CH_4	2.5	15	5825	957
0	CH_4	5.0	10	8669	2138
0	CH_4	10.0	3.9	6754	2443
0	CH_4	20.0	5	38936	20256

0	CH_4	40.0	4.5	107125	59832
0	CD_4	2.9	1	0	0[b]
0	CD_4	5.6	2	16	15[b]
0	CD_4	11.3	17	19808	13736
10	CD_4	11.3	2	3149	2135
20	CD_4	11.3	2	6097	4150
0	CD_4	22.6	10	42368	33007
0	CD_4	45.2	6	68121	54170

[a]Both products have at least their zero-point vibrational energies
[b]No further analysis performed

C. Analysis of Trajectories

Simulating CN + CH_4 collisions to form HCN + CH_3 products helps understand how the potential energy surface and the molecular structures transform collision energy E_{coll} and reaction energy $\Delta E_{reaction}$ into vibrational, rotational, and translation energy in the products. In the analogous experiment, we envision recording velocity-map scattering images of reaction products for various internal states. Thus, for each set of simulated reaction conditions, we sort the successful reactions by their rotational energy and vibrational energy.[18]

We also simulate scattering images of the products. For any given subset, we convert the total kinetic energy released (TKER) to center-of-mass-frame velocities of HCN and CH_3. Collecting scattered products irrespective of azimuthal scattering direction is equivalent to recording a crushed scattering image, so we weight the simulated results by $1/sin\theta$ to extract the central slice, where θ is the deviation angle between the initial CN velocity and the final HCN velocity.

III. Results and Discussion

The full-dimensional EVB surface does a remarkable job of reproducing the *ab initio* surface optimizing relatively few parameters. In **Fig 1**, we compare slices through the two surfaces,

plotting the UCCSD-UHF/aug-cc-pVDZ energies in **panel a** and the EVB surface in **panel b**. Because there are only 230 points in this C_{3v} illustration, with collinear N≡C-H-CH_3 geometries which we use only for presentation in the figure, we have the luxury of using UCCSD-optimized geometries (optimized in all degrees of freedom other than the selected H_3C-H and H-CN distances). The difference between the *ab initio* and EVB energies, shown in **panel c**, highlights the fidelity of the analytical function. By definition, the surfaces have the same energy change, ΔE_0 = -85.4 kJ/mol. Zero-point corrections (see Supporting Information) for reactions with CH_4 give ΔE_{ZPE}^{H}= -93.0 kJ/mol and with CD_4 give ΔE_{ZPE}^{D}= -90.3 kJ/mol . These values agree well with $\Delta_r H_{0\,K}$ = -87 kJ/mol obtained from experimental thermochemistry.[2]

There is a very early barrier to reaction of 9.1 kJ/mol at an extended H_3CH-CN distance of r_{H_3CH-CN} = 1.74 Å and at a reactant-like H_3C-H distance of r_{H_3C-H} = 1.15 Å. The Supporting Information reports further geometric parameters and the harmonic vibrational frequencies of the transition state. At the transition state there is a loss of a high-frequency C-H vibration, decreasing the importance of the barrier in both experiment and a fully quantum-mechanical treatment. Both the barrier height and location are consistent with previous, limited explorations of this surface.[29, 40]

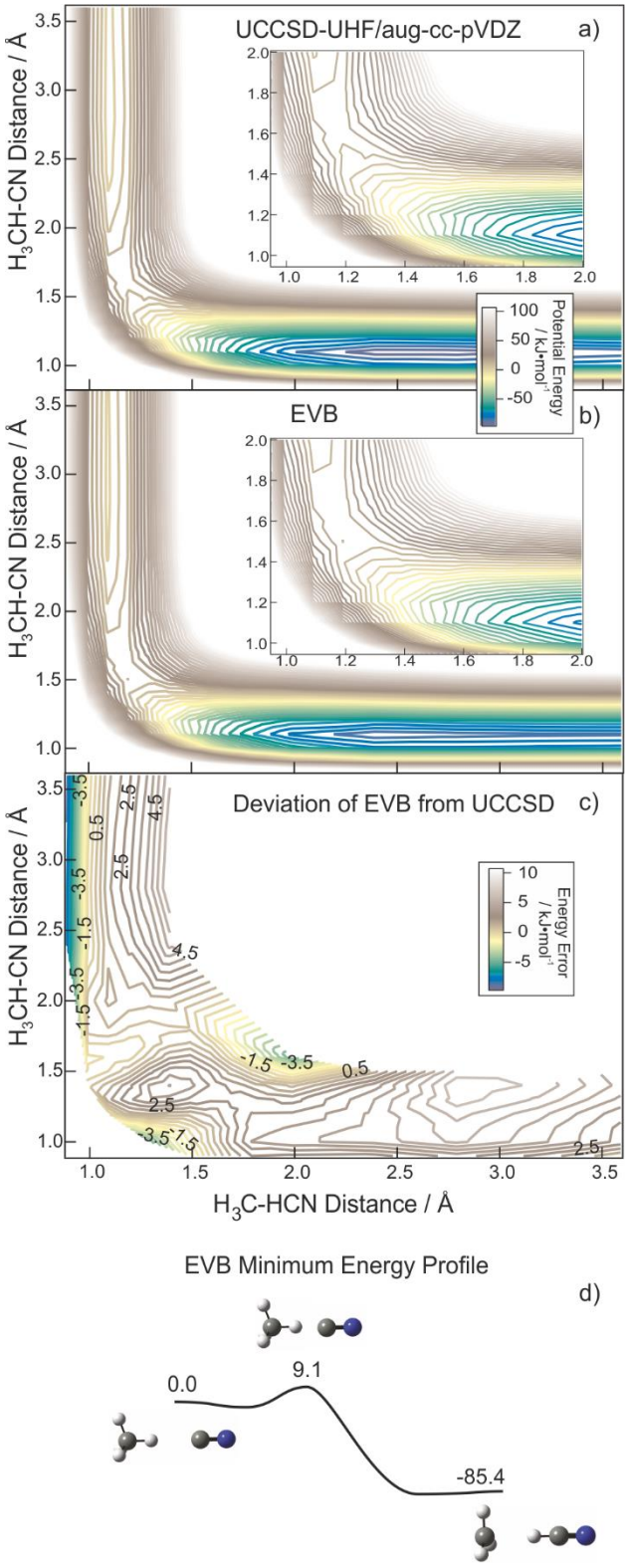

Figure 1. Potential energy surface slices in C_{3v} geometries for CN + CH_4 → HCN + CH_3. The *ab initio* UCCSD-UHF/aug-cc-pVDZ//BB1K/6-31G(d) energies (panel a) use 230 relaxed structures and are drawn with interpolated contours every 5 kJ/mol. The slice through the surface used for trajectory propagation (panel b) has the same molecular geometries as panel a, but uses EVB to calculate energies and has the same energy scale. The grid effect evident in some of the contour lines is an artifact present only in the graph, stems from the interpolation scheme, and is absent in the true EVB and UCCSD surfaces. The error of the EVB energies

relative to the UCCSD energies in the dynamically relevant range is small, and the depiction in panel c has a ten-fold smaller energy range than in panels a and b. Panel d displays the energy profile (with values in kJ/mol) along the EVB minimum energy pathway for the reaction (without zero-point energy corrections).

The surface provides a computationally efficient route to simulate many CN + CH_4 and CN + CD_4 reactions. The results of these simulations are ripe for making comparisons to future experiments and for drawing comparisons beyond results from a bimolecular scattering machine. In this work, we emphasize analysis of the possible observables in a velocity-map ion-imaging experiment, which measures the relative velocity of the scattering fragments as a function of their internal energy. In **Section III d** we explore further how the structured reactants and the surface itself control the dynamics of the title reaction.

a. Collision Efficacy and Opacity

If we are to think of the CN radical as a pseudohalogen, we might surmise that we can use, for example, previous studies of the highly exothermic F + CH_4 → HF + CH_3 reaction to make preliminary assessments of the chemistry in the CN system.[41] A line-of-centers model for the probability of reaction (or reaction cross section σ_R) with collision energy E_{coll} and reaction energy threshold E_{thresh} predicts a (1-E_{thresh}/E_{coll}) dependence. Previous simulation results[41] of the F + CH_4 reaction show reasonable agreement with such an idea. **Figure 2** shows the reaction probability f_{react} versus E_{coll} for CH_4 and CD_4 partners. We calculated f_{react} as the ratio of total zero-point-conserving reactions divided by total simulated collisions; its magnitude is proportional to the reaction cross section σ_R. Data for two subsets of simulations with initially rotationally excited CN fragments at E_{coll} = 11.3 kJ/mol are also included in **Figure 2** to compare the efficacy of rotational and translation energy in promoting reaction.

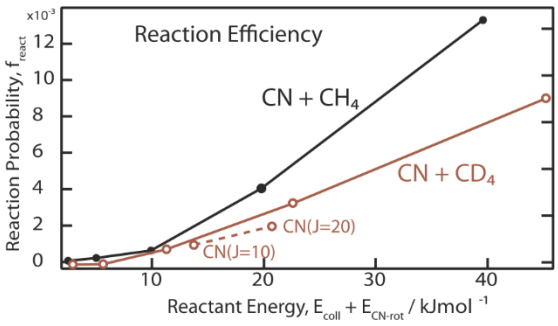

Figure 2. Reaction probability f_{react} for CN + CH_4 → HCN + CH_3 as a function of reactant energy. Each encounter between reactants becomes more likely to generate products as the collision energy increases. A simple line-of-centers model has a concave-down 1-E_{thresh}/E_{coll} dependence, contrary to the observed concave-up trend between methane and the structured CN radical. Statistical uncertainties from the trajectory calculations give error bars smaller than the plotted circles.

The influence of collision energy on f_{react} for both CN + CH_4 and CN + CD_4 differs markedly from the F + CH_4 reaction.[41] The functions are more similar to endothermic Br + CH_4 and O(^{3}P) + CH_4 reactions.[42-44] This curious dependence of f_{react} on E_{coll} indicates that considerations beyond the 2D surface shown in **Figure 1** are necessary to understand the dynamics of the reaction, which involve many degrees of freedom. We believe these changes arise from differences between collisions with anisotropic CN and with spherical atoms. A more thorough description of these ideas appears in **Section III d**.

Long-range forces between the bimolecular reactants can increase the reactive cross section relative to the geometric size of the two species. Geometric and energetic constraints at the point of hydrogen transfer can decrease it. **Figure 3** shows opacity functions *P(b)*, which are the probability distributions of impact parameters *b* that lead to reaction, for each E_{coll}. Each *P(b)* is scaled to have unit area for ease of comparison of their shapes. The opacity functions for H abstraction, shown in **Figure 3a**, are all remarkably similar among all collision energies we study. Head-on collisions (in which the CN approaches the center of mass of the methane) are more likely to lead to reaction than glancing blows. But, glancing blows are more geometrically likely and dominate the overall number of reactive encounters. The aberrant point at the smallest *b* for E_{coll} = 2.5 kJ/mol results from very few reactions at this collision

energy and very few collisions at small *b* - this single data point represents only 4 reactions. The opacity functions *P(b)* for H abstraction are all different from the distributions for D abstraction, shown in **Figure 3b**. Those for H extend to larger *b* and have less curvature. The CN + CD_4 reactions, which propagate on the same surface but differ in atomic masses and initialized zero-point energies, show some amount of inhibition at $b \leq 1.0$ Å. The line-of-centers model for *P(b)* is independent of the transferred mass, but we do not explore further the source of the differences. **Figure 3b** also shows the opacity functions for CN(J=10), with $E_{CN\text{-}rot}$ = 2.5 kJ/mol, and for CN(J=20), with $E_{CN\text{-}rot}$ = 9.4 kJ/mol. At these amounts of excitation, the initial rotational energy in CN has little effect on the shape of the opacity function.

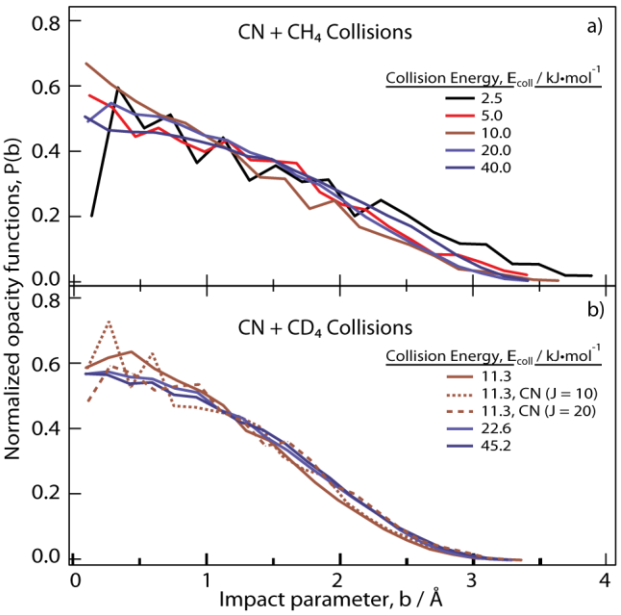

Figure 3. Opacity functions *P(b)* for CN + methane reactions. Panel a shows distributions for CH_4 reactants and panel b shows distributions for CD_4 reactants. The two dashed lines in panel b are for smaller data sets of initially rotationally excited CN fragments.

b. Internal Energy Deposition in Products

The large energy released in the title reaction, $\Delta_r H_{0\ K}$ = -87 kJ/mol, draws our attention for future gas-phase ion-imaging experiments. One aspect of our intention with the current work

is to predict which modes and motions of the products soak up that excess energy. Even at low collision energy, there is enough energy from the reaction to populate up to 2 quanta of C-H stretching vibrations. Previous experimental studies of CN + CH_4 → HCN + CH_3 used photolytic generation of CN in bulk samples,[2] which generates radicals in translationally, rotationally, and vibrationally broad and excited CN distributions. That work showed production of HCN with inverted vibrational distributions, with up to 2 quanta of the C-H stretching mode, and substantial bending excitation. Time-resolved measurements in the liquid phase also use photolytic CN generation to react with larger organic molecules and successfully detect this population inversion in the C-H stretching mode of nascent HCN molecules.[18, 20, 22-24] In a molecular beam, however, we can collisionally cool both reactants before they collide and then interrogate the products under single-collision conditions. Thus, the molecular-beam experiment allows careful control and detection of the energy throughout reaction. We mimic the initial conditions with our simulations and the measurements with our analysis of the simulation results.

There are five motions we consider for energy sinks in the CN + CH_4 reaction (or its fully deuterated analogue): relative total kinetic energy released into the two fragments (*TKER*), methyl rotation ($E_{rot\text{-}CH_3}$), methyl vibration ($E_{vib\text{-}CH_3}$), HCN rotation ($E_{rot\text{-}HCN}$), and HCN vibration ($E_{vib\text{-}HCN}$). We plot in **Figure 4** snapshots of the energy deposited in these product motions for methane. Table II reports mean values of each of these energy distributions for the five collision energies simulated. The Supporting Information shows the corresponding plots and mean product energies for methane-*d4* reactants. For easy comparison across the suite of simulations, each panel of **Figure 4** shows the abscissa as a fraction of total energy available $E_{Avail} = |\Delta E_{ZPE}| + E_{coll}$. Vibrational energies are those in excess of zero-point energy. The fractions of energy in TKER, $E_{vib\text{-}CH_3}$, and $E_{rot\text{-}HCN}$ increase with increasing E_{coll}. The fraction

in $E_{rot\text{-}CH_3}$ is always small and remains unchanged. The fraction decreases for $E_{vib\text{-}HCN}$ with increasing E_{coll}.

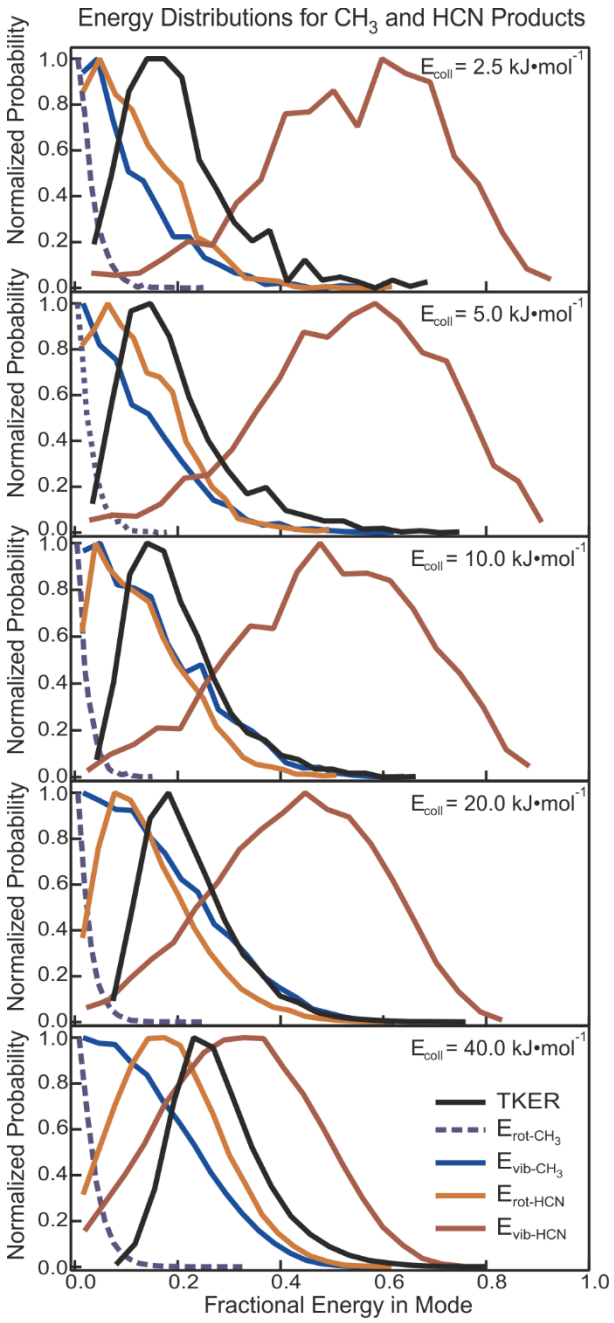

Figure 4. Energy distributions of CN + CH_4 → HCN + CH_3 products for a range of collision energies E_{coll}. The abscissa is the fraction of available energy $E_{Avail} = |\Delta E_{ZPE}| + E_{coll}$ in the particular mode. With increasing E_{coll}, the fraction increases for *TKER* (black line), remains unchanged and small for CH_3 rotations $E_{rot\text{-}CH_3}$ (dashed, dark blue), increases for both CH_3 vibration $E_{vib\text{-}CH_3}$ (light blue) and HCN rotation $E_{rot\text{-}HCN}$ (tan), and decreases for HCN vibration $E_{vib\text{-}HCN}$ (brown). The legend is common to all panels.

TABLE II: Collision Energy Dependence of the Mean Energies in the Various Degrees of Freedom of the Products of the CN + CH_4 Reaction.

	Mean Product Energy [a]				
E_{coll} [a]	CH_3 Rotation	CH_3 Vibration	HCN Rotation	HCN Vibration	Kinetic Energy
2.5	2.3	8.4	9.5	43.8	16.3
5.0	2.1	9.7	10.2	44.7	16.1
10	1.8	12.9	11.6	43.7	17.3
20	2.2	15.7	14.5	42.2	21.8
40	3.5	17.2	22.3	37.7	33.4

[a] All energies are specified in kJ/mol.

Each increase of collision energy allows the system to deviate further from the minimum-energy path. For exothermic atom-diatom A + BC → AB + C reactions, the common notion is for $\Delta E_{reaction}$ to appear as product vibration, which is analogous to C-H stretching in HCN in the present reaction. Excess E_{coll} appears efficiently as product translational and rotational motions.[10, 45] Because all four species in the title reaction, CN, CH_4, HCN, and CH_3, are more complex than their respective A + BC analogues, the current study provides a stringent test of the extension of such elegant ideas to larger chemical systems.

The results shown in **Figure 4** and **Table II** agree, in general, with the atom-diatom trends. Higher E_{coll} deposits more energy in *TKER* (black lines), but to an extent significantly less than predicted by kinematic models for transfer of a light atom.[10] Rotational excitation in the methyl product (dark blue), an unphysical notion in the analogous atomic product C, is independent of the collision energy. The appearance of excess E_{coll} in $E_{vib\text{-}CH_3}$ (light blue) is again an unphysical notion for A + BC, but makes intuitive sense as the collisions become more impulsive with increasing E_{coll}. HCN picks up rotational energy (tan) and decreases its fraction in $E_{vib\text{-}HCN}$ (brown). Even at the lowest E_{coll}, however, nearly all HCN products are vibrationally excited, a common feature of CN + hydrocarbon reactions[1-3, 18, 46] because of their early transition states and large exothermicities, as well as the kinematics of light atom transfer.[10]

Classical trajectories for transfer of a hydrogen atom between two heavier moieties sometimes exhibit oscillatory or "chattering" dynamics in the vicinity of the transition state. Our prior study of the $Cl + C_2H_6 \rightarrow HCl + C_2H_5$ reaction revealed this chattering in fewer than 3% of reactive trajectories, and scattering and kinetic energy release distributions were unaffected.[47-48] We therefore did not look for signatures of this behavior in the current work.

c. Simulated Scattering Images and Product Correlations

The trends shown in **Figure 4** offer a route to critical assessments of the simulations *via* spectroscopic or velocity-mapped ion imaging experiments. Absorptive spectroscopy experiments can measure the product internal energies, similar to previous bulk gas-phase measurements.[1-2, 49] A single imaging experiment can determine the quantum state of one product, the scattering velocity of the products (and thus TKER), and in favorable cases the correlated quantum state of the un-probed product. These scattering experiments are underway in our laboratory and direct our analysis of the simulations.

The four lowest collision energies we simulate correspond to future experiments using counter-propagating and crossing molecular beams, with the reactants entrained in either Ar or He bath gases. **Figure 5** and **Figure 6** show the product scattering maps for various collision energies and product internal energies for HCN from $CN + CH_4$ reactions. The simulations are necessarily left-right symmetric, but we show one full scattering image for the highest collision energy in **Figure 5**.

The simulated images in **Figure 5** gather up all products, irrespective of internal energy (i.e. without quantum state selectivity). Each panel represents a different number of reactive events, as listed in **Table I**. Backward scattering, which we define as HCN departing to the same hemisphere as CN started (or, equivalently, methyl departing to the same hemisphere as methane started), is prominent at all collision energies. Increasing E_{coll} opens up the forward

hemisphere to reactive scattering, as shown by the progression from bottom to top in Figure 5. These forward-scattering events arise because glancing blows at large impact parameter become reactive, analogous to many halogen + CH_4 collisions.[42, 50] We show in **Figures 4 and 5** that the HCN formed in the reaction is vibrationally excited, consistent with experimental measurements.[2] Maximum product speeds for different numbers of quanta in the C-H mode of HCN are given as clipped dotted circles. The limits for vibrationless products are beyond the graphical range of the figure. These scattering images are complementary to the distributions plotted in **Figure 4**. The maps for methane-*d4* are similar and appear in the Supporting Information.

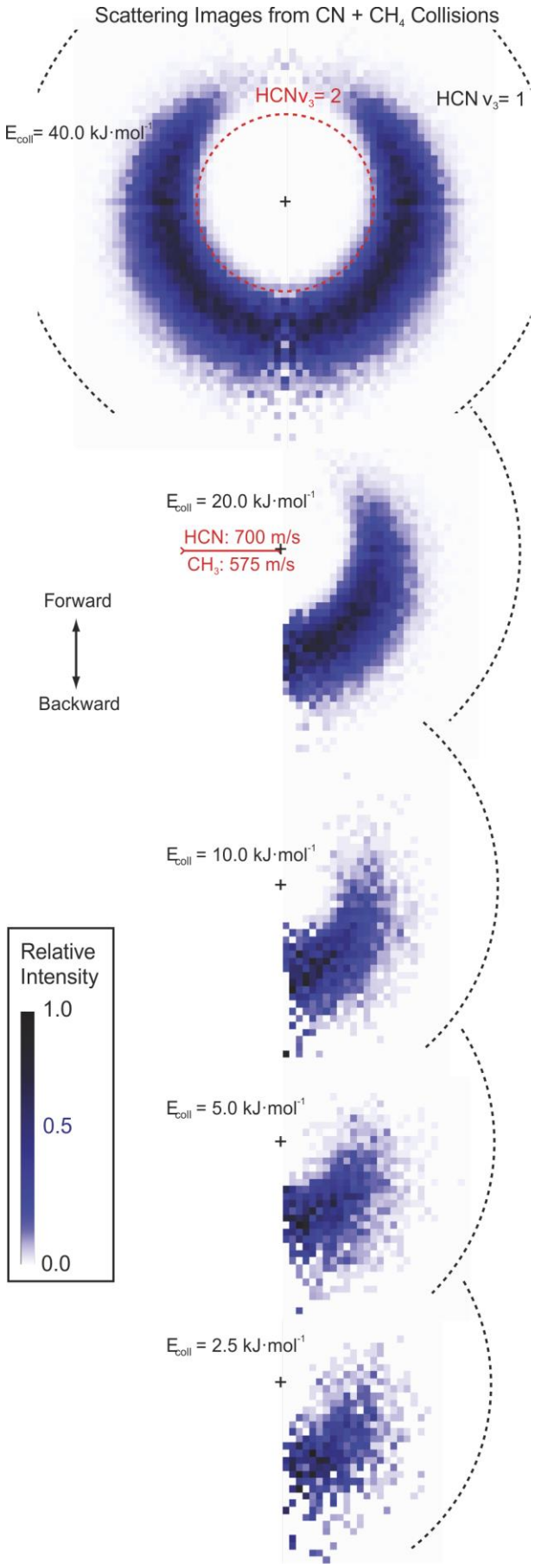
Scattering Images from CN + CH4 Collisions
HCN v3= 2
HCN v3= 1
Ecoll= 40.0 kJ·mol-1
Ecoll = 20.0 kJ·mol-1
HCN: 700 m/s
CH3: 575 m/s
Forward
Backward
Ecoll = 10.0 kJ·mol-1
Ecoll = 5.0 kJ·mol-1
Ecoll = 2.5 kJ·mol-1
Relative Intensity
1.0
0.5
0.0

Figure 5. Simulated images for CN + CH_4 → HCN + CH_3 products. Products scatter predominantly in the backward hemisphere. Sideways and forward scattering become more prominent as the collision energy E_{coll} increases. All images use the same (arbitrary) linear color scale. The pixel-to-velocity scale (given by two scale bars) depends on the choice of the detected product and is the same for all images. The "+" in the images marks 0 m/s in the molecular frame of reference. The dotted lines denote maximum speeds for each given number of C-H stretching quanta in HCN, corresponding to no excitation in CH_3 or the other HCN vibrational modes.

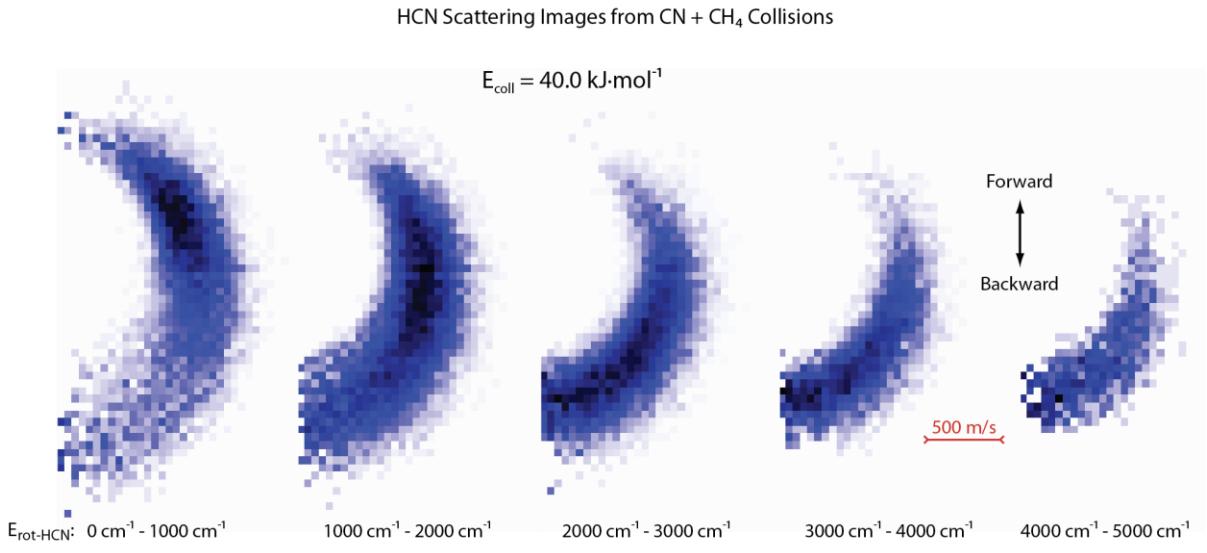

Figure 6. Scattering distributions for HCN from CN + CH_4 → HCN + CH_3, shown separated by HCN rotational energy. Rotationally cold HCN fragments scatter forward, rotational excitation favors the backward hemisphere.

The amount of rotational energy in the products is smaller in the forward hemisphere, as displayed in **Figure 6**. The trend is in concert with halogen + CH_4 collisions (see Ref. [42], for example.) The series of images in **Figure 6** emulates the ability of velocity-mapped measurements coupled with state-selective ionization to capture correlations in the reaction properties. In this case, the scattering angle θ is anti-correlated with HCN rotational energy $E_{HCN\text{-}rot}$. We calculate the correlation coefficients of several properties for each E_{coll} and show the results for E_{coll} = 40.0 kJ·mol^{-1} pictorially in the **top panel** of **Figure 7**. The correlations are a function of the collision energy, and the **bottom panel** of **Figure 7** shows the evolution of a few selected correlation coefficients with E_{coll}. Many scattering properties become more

coupled with increasing collision energy. The set of the evolving correlation coefficients with E_{coll} appears in the Supporting Information.

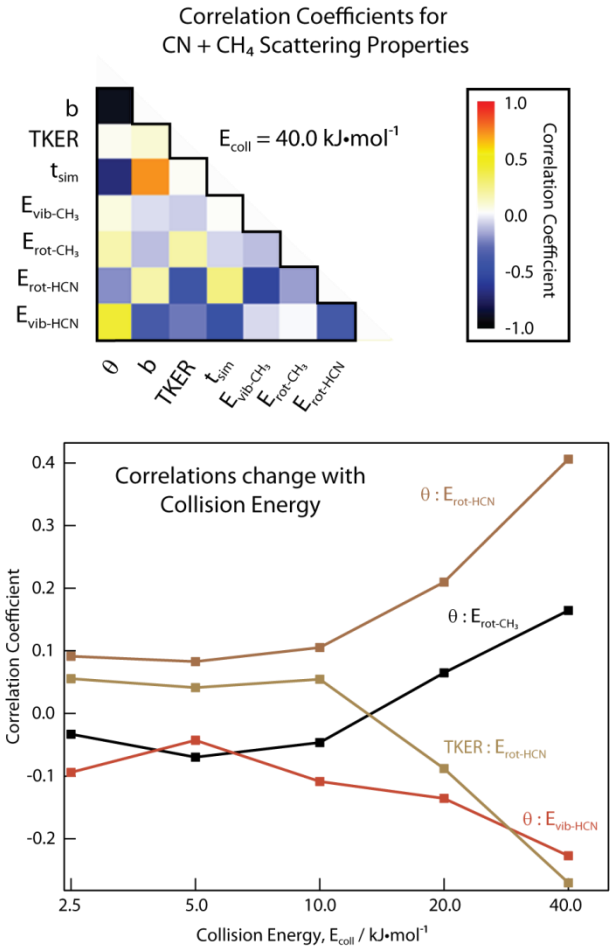

Figure 7. Correlation coefficients for several properties of CN + CH_4 → HCN + CH_3 simulations. The top panel shows the coefficients for the highest collision energy we simulate, E_{coll} = 40.0 kJ·mol^{-1}. The bottom panel shows the evolution of selected coefficients with E_{coll}. Abbreviations are as follows: θ - scattering angle between initial CN and final HCN velocities, *b* - impact parameter, *TKER* - total kinetic energy released, t_{sim} - simulation (or reaction) time, $E_{vib\text{-}CH_3}$ - methyl vibrational energy, $E_{rot\text{-}CH_3}$ - methyl rotational energy, $E_{rot\text{-}HCN}$ - HCN rotational energy, $E_{vib\text{-}HCN}$ - HCN vibrational energy.

d. Influence of Diatomic Collider

The reaction cross section σ_R deviates from a (1-E_{thresh}/E_{coll}) functional form, as shown in **Figure 2**. To inspect its cause, we explore the idea of the angle of the cone of acceptance, a limited, but convenient, mathematical descriptor for steric hindrance.[10, 51] For a monatomic

collider X with CH_4, γ is the deviation of the X-H-CH_3 angle from 180°. The barrier to reaction, or threshold energy E_{thresh}, depends on γ, and we write $E_{thresh} = E_{thresh}(\cos\gamma)$.[10] Successful reactions are those with $E_{coll} > E_{thresh}(\cos\gamma)$; thus γ defines the angles available for reaction - the cone of acceptance. For the diatomic collider, we similarly define γ as the deviation of the H_3C-H-CN angle from 180°. The potential is relatively insensitive to modest deviations of γ. A flat potential near $\gamma = 0°$ has two immediate consequences: one, minimal torque to reorient the CN radical during the collision, and, two, a large cone of acceptance.[10]

The angle γ, however, does not sufficiently define the orientation of CN with respect to the H_3C-H bond. The minimum energy path involves collinear approach of the CN radical to the C-H bond, but approach with a partially side-on CN radical can contribute increasingly to reactivity with increasing collision energy. This CN radical orientation dependence adds a second degree of freedom to the cone-of-acceptance idea for an atomic collider. We use a second angle ϕ to denote the deviation of the H_3CH-C-N angle from 180°. A dihedral angle is also required to uniquely orient the C-N vector, but in the present analysis we assume the energy about this angle is isotropic and integrates out as does ϕ for a monatomic collider.[10] In the entrance channel, at long H_3CH-CN distances, the potential is insensitive to ϕ, as shown in **panel a** of **Figure 8**. In the Figure, we plot the energy for $\phi = 30°$ minus the energy for $\phi = 0°$. There is little torque on CN along ϕ, as is the case in the coordinate γ, prior to reaction. Only after reaching the H-transfer region does ϕ affect the potential. In this case, the system with $\phi = 30°$ requires an extra 30 kJ/mol in the appropriate degree of freedom to react. A graphical definition of γ and ϕ is shown in the inset of **Figure 8**.

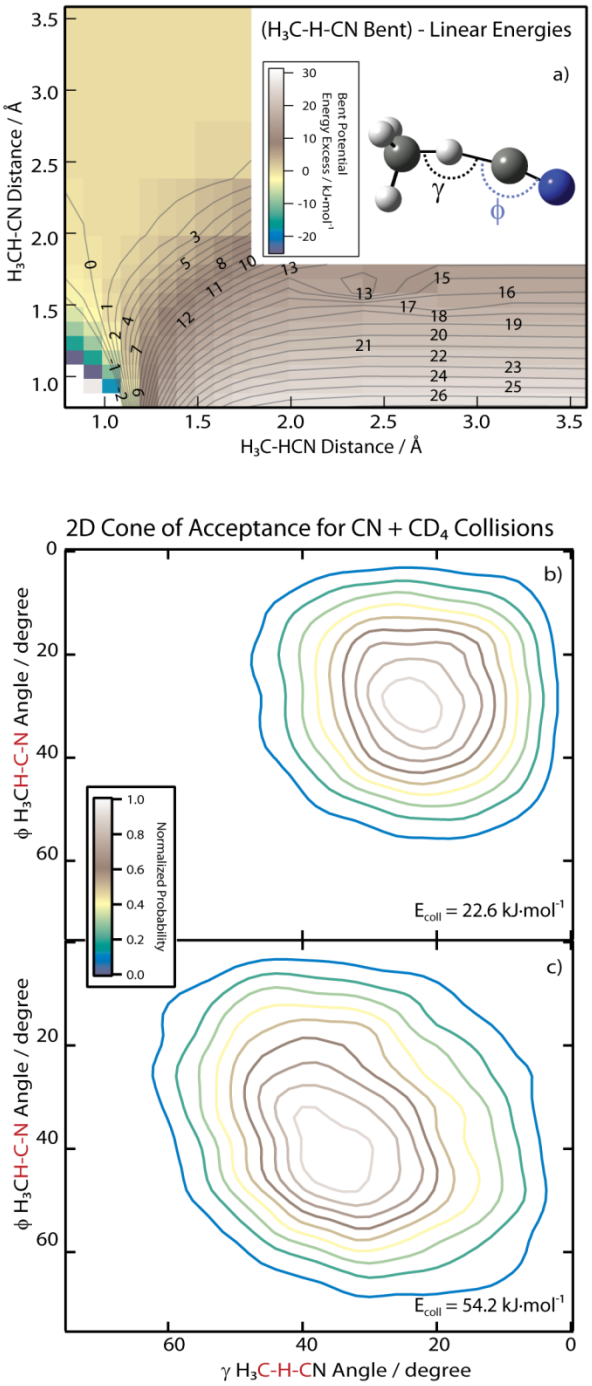

Figure 8. Understanding the role of the structured CN radical on CN + methane reaction dynamics. Bending the N atom away from the C_{3v} axis does not affect the potential energy until the hydrogen-transfer region. Panel a shows the excess potential energy for $\phi = 30°$ relative to $\phi = 0°$. Panel b shows the distribution of γ and ϕ at the point of D transfer for CN + CD_4 collisions at E_{coll} = 22.6 kJ·mol^{-1}. Panel c shows their distributions at E_{coll} = 45.2 kJ·mol^{-1}. These distributions were obtained from trajectories with impact parameters $b \leq 1$ Å. Low geometric probability of CN colliding in collinear D_3C-D-C-N geometries shifts the distribution of γ and ϕ for reactions away from 0°, their values on the minimum-energy path. Increasing E_{coll} opens up the two-dimensional cone of acceptance. The data in panels b and c have been smoothed for clarity.

The probabilities for the two independent constraints γ and ϕ to be within their own reactive ranges multiply together, decreasing the reaction rate. The largest ratio of $\sigma_R/\pi b_{max}^2$ we determine for CN + CD_4 → DCN + CD_3 is about 0.01 (cf. **Figure 2**) where $E_{coll} > 3 \cdot E_{thresh.}$ To provide a better handle on these constraints, we extract two-dimensional distributions of γ and ϕ for simulated CN + CD_4 reactions with 0.0 Å ≤ b ≤ 1.0 Å for E_{coll} = 22.6 kJ·mol^{-1} in **panel b** and for E_{coll} = 45.2 kJ·mol^{-1} in **panel c** of **Figure 8**. The distribution shifts to more linear configurations if we choose to use all b, but we find low-impact parameters more intuitive to envisage. For these plots, γ and ϕ are calculated when the D_3C-D bond distance extends to 1.3 Å. Different cutoff distances slightly change the center of the distribution of γ and ϕ, but our interpretation is the same over a reasonable range of choices.

As the collision energy increases, so too do the breadth of angles ϕ and γ that lead to reaction. With a monatomic collider, the line-of-centers model predicts a region of concave-up dependence on $\sigma_R(E_{coll})$ whose range scales with bending stiffness of the potential along γ, E'_{thresh}. Once $E_{coll} > E_{thresh} + 2E'_{thresh}$, $\sigma_R(E_{coll})$ takes a concave-down dependence.[10] With the diatomic collider, the concave-up region depends on the derivative of *both* angles ϕ and γ, inhibiting the turnover as shown in **Figure 2**.

The difference between panels b and c of **Figure 8** shows how these two dimensions still work in concert to enhance the reaction cross section σ_R well above E_{thresh}. The minimum-energy path goes through $\gamma = 0°$, $\phi = 0°$. The probability distributions in the figure thus signify the action of the geometric probabilities of γ and ϕ on the potential energy surface. The delayed opening of the two-dimensional cone-of-acceptance produces the concave-up trend presented in **Figure 2**, in parallel with X + CH_4 collisions. Thus much of the powerful intuition that we gain by following a line-of-centers approach to bimolecular collisions holds even with more complicated colliders, but we must be aware of new restrictions imposed by non-spherical

reaction partners which impose their own orientation dependence on the reaction dynamics. The CN-radical orientation dependence is particularly pronounced because the weak angular anisotropy in the reactants' side of the PES does not promote reorientation to a favorable reactive geometry.

IV. Outlook and Conclusions

The new CN + CH_4 → HCN + CH_3 surface we present uses the empirical valence bonding method[30-31] to provide an analytical description for efficient trajectory propagation. The full-dimensional surface closely matches the 770 energies from UCCSD-UHF/aug-cc-pVDZ calculations used for fitting and it agrees well with previous experimental[2, 25] and computational[29, 40] assessments. The quasi-classical trajectory results produce vibrationally excited HCN, as in experiment.[2] Increasing collision energy deposits excess energy into relative product translation. Both outcomes agree with Polanyi's rules for atom-diatom A + BC → AB + C reactions.[45] Many ideas still carry through to CN + CH_4, even though each species in the title reaction is more complex than its analogue in A + BC collisions. Simulated velocity-map images of the products provide stringent tests of the surface by future experiments.

Diatomic CN brings with it geometric constraints not present in atoms. We explore the idea of a cone of acceptance for the pseudohalogen, but add a second dimension to define the CN orientation as is collides with methane. The fundamental ideas of the line-of-centers model still hold, but the anisotropy of CN creates a broader window of collision energies over which the cone of acceptance dominates reaction probability.

Acknowledgement

This work is supported by EPSRC Programme Grant EP/L005913/1. SP acknowledges the University of Bristol for a postgraduate scholarship.

Supporting Information Description

Descriptions and assessments of EVB potential energy surface. Energy partitioning and simulated scattering images for CN + CD_4 reactions. Correlation coefficients for CN + CH_4 and CN + CD_4 for each collision energy. This information is available free of charge via the Internet at http://pubs.acs.org

References

1. Bethardy, G. A.; Northrup, F. J.; Macdonald, R. G. The Initial Vibrational-State Distribution of HCN $X^1\Sigma^+$ (v_1,0,v_3) from the Reaction CN($^2\Sigma^+$)+$C_2H_6 \rightarrow$ HCN+C_2H_5. *J. Chem. Phys.* **1995,** *102*, 7966-7982.
2. Bethardy, G. A.; Northrup, F. J.; Macdonald, R. G. The Initial Vibrational Level Distribution and Relaxation of HCN $X^1\Sigma^+$ (v_1,0,v_3) in the CN($^2\Sigma^+$)+$CH_4 \rightarrow$ HCN+CH_3 Reaction System. *J. Chem. Phys.* **1996,** *105*, 4533-4549.
3. Copeland, L. R.; Mohammad, F.; Zahedi, M.; Volman, D. H.; Jackson, W. M. Rate Constants for CN Reactions with Hydrocarbons and the Product HCN Vibrational Populations: Examples of Heavy-Light-Heavy Abstraction Reactions. *J. Chem. Phys.* **1992,** *96*, 5817-5826.
4. Huang, C.; Li, W.; Estillore, A. D.; Suits, A. G. Dynamics of CN Plus Alkane Reactions by Crossed-Beam Dc Slice Imaging. *J. Chem. Phys.* **2008,** *129*, 074301.
5. Yang, D. L.; Lin, M. C. The Reactions of the CN Radical with Molecules Relevant to Combustion and Atmospheric Chemistry. In *The Chemical Dynamics and Kinetics of Small Radicals, Part I*, Liu, K.; Wagner, A., Eds. World Scientific: Singapore, 1995; pp 164-213.
6. Abeysekera, C.; Joalland, B.; Ariyasingha, N.; Zack, L. N.; Sims, I. R.; Field, R. W.; Suits, A. G. Product Branching in the Low Temperature Reaction of CN with Propyne by Chirped-Pulse Microwave Spectroscopy in a Uniform Supersonic Flow. *J Phys Chem Lett* **2015,** *6*, 1599-1604.
7. Estillore, A. D.; Visger, L. M.; Kaiser, R. I.; Suits, A. G. Crossed-Beam Imaging of the H Abstraction Channel in the Reaction of CN with 1-Pentene. *J. Phys. Chem. Lett.* **2010,** *1*, 2417-2421.
8. Parr, R. G.; Von Szentpaly, L.; Liu, S. B. Electrophilicity Index. *J Am Chem Soc* **1999,** *121*, 1922-1924.
9. Liu, K. Vibrational-Induced Steric Effects in Bimolecular Reactions. *J. Chem. Phys.* **2015,** *142*, 080901.
10. Levine, R. D. *Molecular Reaction Dynamics*. Cambridge University Press: Cambridge, 2005.
11. Orr-Ewing, A. J. Dynamical Stereochemistry of Bimolecular Reactions. *J Chem Soc Faraday T* **1996,** *92*, 881-900.
12. Hornung, B.; Harvey, J. N.; Preston, T. J.; Dunning, G. T.; Orr-Ewing, A. J. Empirical Valence Bond Theory Studies of the CH_4 + Cl $\rightarrow$ CH_3 + HCl Reaction. *J. Phys. Chem. A* **2015,** *119*, 9590 - 9598.

13. Preston, T. J.; Dunning, G. T.; Orr-Ewing, A. J.; Vazquez, S. A. Direct and Indirect Hydrogen Abstraction in Cl + Alkene Reactions. *J. Phys. Chem. A* **2014,** *118*, 5595-5607.
14. Hornung, B.; Preston, T. J.; Pandit, S.; Harvey, J. N.; Orr-Ewing, A. J. Computational Study of Competition between Direct Abstraction and Addition-Elimination in the Reaction of Cl Atoms with Propene. *J. Phys. Chem. A* **2015,** *119*, 9452 - 9464.
15. Abou-Chahine, F.; Greaves, S. J.; Dunning, G. T.; Orr-Ewing, A. J.; Greetham, G. M.; Clark, I. P.; Towrie, M. Vibrationally Resolved Dynamics of the Reaction of Cl Atoms with 2,3-Dimethylbut-2-Ene in Chlorinated Solvents. *Chem. Sci.* **2013,** *4*, 226-237.
16. Dunning, G. T.; Glowacki, D. R.; Preston, T. J.; Greaves, S. J.; Greetham, G. M.; Clark, I. P.; Towrie, M.; Harvey, J. N.; Orr-Ewing, A. J. Vibrational Relaxation and Microsolvation of DF after F-Atom Reactions in Polar Solvents. *Science* **2015,** *347*, 530-533.
17. Dunning, G. T.; Murdock, D.; Greetham, G. M.; Clark, I. P.; Orr-Ewing, A. J. Solvent Response to Fluorine-Atom Reaction Dynamics in Liquid Acetonitrile. *Phys. Chem. Chem. Phys.* **2015,** *17*, 9465-9470.
18. Glowacki, D. R.; Orr-Ewing, A. J.; Harvey, J. N. Product Energy Deposition of CN + Alkane H Abstraction Reactions in Gas and Solution Phases. *J. Chem. Phys.* **2011,** *134*, 214508-11.
19. Glowacki, D. R.; Rose, R. A.; Greaves, S. J.; Orr-Ewing, A. J.; Harvey, J. N. Ultrafast Energy Flow in the Wake of Solution-Phase Bimolecular Reactions. *Nat. Chem.* **2011,** *3*, 850-855.
20. Greaves, S. J.; Rose, R. A.; Oliver, T. A. A.; Glowacki, D. R.; Ashfold, M. N. R.; Harvey, J. N.; Clark, I. P.; Greetham, G. M.; Parker, A. W.; Towrie, M., et al. Vibrationally Quantum-State-Specific Reaction Dynamics of H Atom Abstraction by CN Radical in Solution. *Science* **2011,** *331*, 1423-1426.
21. Orr-Ewing, A. J.; Glowacki, D. R.; Greaves, S. J.; Rose, R. A. Chemical Reaction Dynamics in Liquid Solutions. *J. Phys. Chem. Lett.* **2011,** *2*, 1139-1144.
22. Rose, R. A.; Greaves, S. J.; Abou-Chahine, F.; Glowacki, D. R.; Oliver, T. A. A.; Ashfold, M. N. R.; Clark, I. P.; Greetham, G. M.; Towrie, M.; Orr-Ewing, A. J. Reaction Dynamics of CN Radicals with Tetrahydrofuran in Liquid Solutions. *Phys. Chem. Chem. Phys.* **2012,** *14*, 10424-10437.
23. Rose, R. A.; Greaves, S. J.; Oliver, T. A. A.; Clark, I. P.; Greetham, G. M.; Parker, A. W.; Towrie, M.; Orr-Ewing, A. J. Vibrationally Quantum-State-Specific Dynamics of the Reactions of CN Radicals with Organic Molecules in Solution. *J. Chem. Phys.* **2011,** *134*, 244503.
24. Dunning, G. T.; Preston, T. J.; Greaves, S. J.; Greetham, G. M.; Clark, I. P.; Orr-Ewing, A. J. Vibrational Excitation of Both Products of the Reaction of CN Radicals with Acetone in Solution. *J. Phys. Chem. A* **2015**, *119*, 12090-12101.
25. Sims, I. R.; Queffelec, J. L.; Travers, D.; Rowe, B. R.; Herbert, L. B.; Karthauser, J.; Smith, I. W. M. Rate Constants for the Reactions of CN with Hydrocarbons at Low and Ultra-Low Temperatures. *Chem Phys Lett* **1993,** *211*, 461-468.
26. Balucani, N.; Asvany, O.; Chang, A. H. H.; Lin, S. H.; Lee, Y. T.; Kaiser, R. I.; Bettinger, H. F.; Schleyer, P. V.; Schaefer, H. F. Crossed Beam Reaction of Cyano Radicals with Hydrocarbon Molecules. I. Chemical Dynamics of Cyanobenzene (C_6H_5CN; X^1A_1) and Perdeutero Cyanobenzene (C_6D_5CN; X^1A_1) Formation from Reaction of $CN(X\ ^2\Sigma^+)$ with Benzene $C_6H_6(X^1A_{1g})$, and d_6-Benzene $C_6D_6(X^1A_{1g})$. *J Chem Phys* **1999,** *111*, 7457-7471.
27. Balucani, N.; Asvany, O.; Chang, A. H. H.; Lin, S. H.; Lee, Y. T.; Kaiser, R. I.; Bettinger, H. F.; Schleyer, P. V.; Schaefer, H. F. Crossed Beam Reaction of Cyano Radicals with Hydrocarbon Molecules. II. Chemical Dynamics of 1-Cyano-1-Methylallene

($CNCH_3CCCH_2$; X^1A') Formation from Reaction of $CN(X\ ^2\Sigma^+)$ with Dimethylacetylene CH_3CCCH_3 ($X\ ^1A_1'$). *J Chem Phys* **1999,** *111*, 7472-7479.
28. Leonori, F.; Petrucci, R.; Wang, X. A.; Casavecchia, P.; Balucani, N. A Crossed Beam Study of the Reaction CN + C_2H_4 at a High Collision Energy: The Opening of a New Reaction Channel. *Chem Phys Lett* **2012,** *553*, 1-5.
29. Yang, D. L.; Yu, T.; Lin, M. C.; Melius, C. F. The Reaction of CN with CH_4 and CD_4 - an Experimental and Theoretical-Study. *Chem Phys* **1993,** *177*, 271-280.
30. Warshel, A.; Weiss, R. M. An Empirical Valence Bond Approach for Comparing Reactions in Solutions and in Enzymes. *J Am Chem Soc* **1980,** *102*, 6218-6226.
31. Chang, Y. T.; Miller, W. H. An Empirical Valence Bond Model for Constructing Global Potential-Energy Surfaces for Chemical-Reactions of Polyatomic Molecular-Systems. *J Phys Chem-US* **1990,** *94*, 5884-5888.
32. Glowacki, D. R.; Orr-Ewing, A. J.; Harvey, J. N. Non-Equilibrium Reaction and Relaxation Dynamics in a Strongly Interacting Explicit Solvent: F + CD_3CN Treated with a Parallel Multi-State EVB Model. *J. Chem. Phys.* **2015,** *143*, 044120.
33. Gutierrez-Oliva, S.; Diaz, S.; Toro-Labbe, A.; Lane, P.; Murray, J. S.; Politzer, P. Revisiting the Seemingly Straightforward Hydrogen Cyanide/Hydrogen Isocyanide Isomerisation. *Mol Phys* **2014,** *112*, 349-354.
34. Van Dine, G. W.; Hoffmann, R. Isocyanide-Cyanide and Isoelectronic Rearrangements. *J. Am. Chem. Soc.* **1968,** *90*, 3227-3232.
35. Frisch, M. J.; Trucks, G. W.; Schlegel, H. B.; Scuseria, G. E.; Robb, M. A.; Cheeseman, J. R.; Scalmani, G.; Barone, V.; Mennucci, B.; Petersson, G. A., et al. *Gaussian 09*, Gaussian Inc., Wallingford CT, 2009.
36. Buckingham, R. A.; Corner, J. Tables of 2nd Virial and Low-Pressure Joule-Thomson Coefficients for Intermolecular Potentials with Exponential Repulsion. *Proc R Soc Lon Ser-A* **1947,** *189*, 118-129.
37. Hase, W. L.; Duchovic, R. J.; Hu, X.; Komornicki, A.; Lim, K. F.; Lu, D.-H.; Peslherbe, G. H.; Swamy, K. N.; Vande Linde, S. R.; Varandas, A. J. C., et al. *Venus96: A General Chemical Dynamics Computer Program*, 1996.
38. Hu, X. C.; Hase, W. L.; Pirraglia, T. Vectorization of the General Monte-Carlo Classical Trajectory Program Venus. *J. Comput. Chem.* **1991,** *12*, 1014-1024.
39. Lourderaj, U.; Sun, R.; Kohale, S. C.; Barnes, G. L.; de Jong, W. A.; Windus, T. L.; Hase, W. L. The Venus/NWCHEM Software Package. Tight Coupling between Chemical Dynamics Simulations and Electronic Structure Theory. *Comput. Phys. Commun.* **2014,** *185*, 1074-1080.
40. Rao, V. S.; Chandra, A. K. Reactions of Cyanogen Radical with Alkanes and an Explanation for Negative Temperature-Dependence of Rate Constants. *Chem Phys* **1995,** *192*, 247-254.
41. Czako, G.; Bowman, J. M. An Ab Initio Spin-Orbit-Corrected Potential Energy Surface and Dynamics for the F + CH_4 and F + CHD_3 Reactions. *Phys Chem Chem Phys* **2011,** *13*, 8306-8312.
42. Czako, G.; Bowman, J. M. Reaction Dynamics of Methane with F, O, Cl, and Br on Ab Initio Potential Energy Surfaces. *J Phys Chem A* **2014,** *118*, 2839-2864.
43. Czako, G.; Bowman, J. M. Dynamics of the $O(^3P)$ + CHD_3(v(CH)=0,1) Reactions on an Accurate Ab Initio Potential Energy Surface. *P Natl Acad Sci USA* **2012,** *109*, 7997-8001.
44. Czako, G.; Liu, R.; Yang, M. H.; Bowman, J. M.; Guo, H. Quasiclassical Trajectory Studies of the $O(^3P)+CX_4(v_k=0, 1) \rightarrow OX(v)+CX_3(n_1n_2n_3n_4)$ [X = H and D] Reactions on an Ab Initio Potential Energy Surface. *J Phys Chem A* **2013,** *117*, 6409-6420.
45. Polanyi, J. C. Concepts in Reaction Dynamics. *Acc. Chem. Res.* **1972,** *5*, 161-168.

46. Few, J. FTIR Studies of Chemical Processes. D.Phil. Thesis, University of Oxford, 2013.
47. Greaves, S. J.; Orr-Ewing, A. J.; Troya, D. Classical Trajectory Study of the Dynamics of the Reaction of Cl Atoms with Ethane. *J. Phys. Chem. A* **2008,** *112*, 9387-9395.
48. Greaves, S. J.; Kim, J.; Orr-Ewing, A. J.; Troya, D. Studying 'Chattering Collisions' in the Cl Plus Ethane Reaction with Classical Trajectories. *Chem Phys Lett* **2007,** *441*, 171-175.
49. Bethardy, G. A.; Northrup, F. J.; He, G.; Tokue, I.; Macdonald, R. G. Initial Vibrational Level Distribution of HCN[$X^1\Sigma^+$ (v_1,0,v_3)] from the CN($X^2\Sigma^+$)+$H_2 \rightarrow$ HCN+H Reaction. *J. Chem. Phys.* **1998,** *109*, 4224-4236.
50. Zhang, B. L.; Liu, K. P.; Czako, G.; Bowman, J. M. Translational Energy Dependence of the Cl + CH_4(ν_b=0, 1) Reactions: A Joint Crossed-Beam and Quasiclassical Trajectory Study. *Mol Phys* **2012,** *110*, 1617-1626.
51. Blais, N. C.; Bernstein, R. B.; Levine, R. D. Orientation Dependence of the H + D_2 Reaction Cross-Section - Steric Model vs Trajectory Calculations. *J Phys Chem-US* **1985,** *89*, 10-13.

Table of Contents Graphic